npj Quantum Information

https://doi.org/10.1038/s41534-025-01145-3

Article in Press

Quantum circuit for non-unitary linear transformation of basis sets

Received: 26 May 2025

Accepted: 11 November 2025

Cite this article as: Zhu, G., Bierman, J., Lu, J. *et al.* Quantum circuit for non-unitary linear transformation of basis sets. *npj Quantum Inf* (2025). https://doi.org/10.1038/s41534-025-01145-3

Guorui Zhu, Joel Bierman, Jianfeng Lu & Yingzhou Li

We are providing an unedited version of this manuscript to give early access to its findings. Before final publication, the manuscript will undergo further editing. Please note there may be errors present which affect the content, and all legal disclaimers apply.

If this paper is publishing under a Transparent Peer Review model then Peer Review reports will publish with the final article.

ARTICLE IN PRESS

© The Author(s) 2025. **Open Access** This article is licensed under a Creative Commons Attribution-NonCommercial-NoDerivatives 4.0 International License, which permits any non-commercial use, sharing, distribution and reproduction in any medium or format, as long as you give appropriate credit to the original author(s) and the source, provide a link to the Creative Commons licence, and indicate if you modified the licensed material. You do not have permission under this licence to share adapted material derived from this article or parts of it. The images or other third party material in this article are included in the article's Creative Commons licence, unless indicated otherwise in a credit line to the material. If material is not included in the article's Creative Commons licence and your intended use is not permitted by statutory regulation or exceeds the permitted use, you will need to obtain permission directly from the copyright holder. To view a copy of this licence, visit http://creativecommons.org/licenses/by-nc-nd/4.0/.

ARTICLE IN PRESS

Quantum Circuit for Non-Unitary Linear Transformation of Basis Sets

Guorui Zhu[1], Joel Bierman[2], Jianfeng Lu[3,*], and Yingzhou Li[1,4,5,*]
[1]*School of Mathematical Sciences, Fudan University, Shanghai 200433, China*
[2]*Department of Physics, Duke University, Durham, NC 27708, USA*
[3]*Departments of Mathematics, Physics, and Chemistry, Duke University, Durham, NC 27708, USA*
[4]*School of Mathematical Sciences, Shanghai Key Laboratory for Contemporary Applied Mathematics, Fudan University, Shanghai 200433, China and*
[5]*Key Laboratory of Computational Physical Sciences, Ministry of Education, Shanghai 200438, China**

ABSTRACT

This paper presents a novel approach for implementing non-unitary basis transformations on quantum computational platforms, extending beyond conventional unitary methods. By integrating Singular Value Decomposition (SVD), the method achieves operational depth $O(n)$ with about n ancilla qubits, enhancing the analysis of fermionic systems. The non-unitary transformation enables mapping a wavefunction between different bases, allowing the calculation of overlaps of states residing in distinct Hilbert subspaces. This capability supports the use of state-specific ansatzes to compute multiple energy eigenstates under orbital-optimized settings, potentially improving accuracy in variational quantum eigensolver (VQE) and related frameworks. Overall, the method expands the range of accessible quantum states and phenomena, offering new opportunities for applying quantum computing in physics and chemistry.

INTRODUCTION

Solving many-body Schrödinger equation is one of the most promising applications on quantum computers, especially in the era of noisy intermediate-scale and early fault-tolerant quantum computing. Quantum algorithms that could be applied to solve the many-body Schrödinger equation include but not limited to variational quantum algorithms (VQAs) [1–4], quantum phase estimation (QPE) [5–8], quantum simulation [9], etc. While there exist multiple approaches for simulating quantum chemistry on digital quantum computers—including first-quantization schemes and more analog evolution methods—here we focus on the approach in which the many-body Schrödinger equation is discretized on a chosen basis set, with the resulting operator and wavefunction represented as a quantum circuit and a quantum state, respectively.

Throughout the computation, when a change of basis set is performed, i.e., a linear transformation of the basis set, we could either recalculate coefficients on classical computer and restart the quantum algorithm, or carry out the linear transformation via a quantum circuit. Implementing quantum circuit for the linear transformation is mandatory under various scenarios, e.g., calculating the inner product between two many-body wavefunctions discretized by different basis sets. When two basis sets are unitary linear transformations of each other, the corresponding linear transformation is unitary and the quantum circuit has been studied in [10–12]. When two basis sets are not unitary linear transformations of each other, the corresponding linear transformation is non-unitary, for which the quantum circuit implementation is proposed by this paper.

Unitary linear transformation of basis set plays an important role in quantum physics and chemistry. Hartree-Fock method [13–19] looks for the optimal unitary linear transformation of basis set such that the single Slater determinant minimizes the energy of the many-body Hamiltonian operator. Unitary linear transformations of basis set are also used widely in basis set optimization methods, e.g., natural orbital rotation [15–19], complete active space self-consistent field method (CASSCF) [20–34], optimal orbital full configuration interaction (OptOrbFCI) [35], etc. Such unitary linear transformations of basis sets are combined with quantum algorithms for ground state calculation [36–39] to boost the power of quantum computer and pursuing the infinite basis set limit. The unitary linear basis transformation can also be adopted in quantum algorithms for excited states calculation [37, 38, 40] as long as they use the same basis set to represent both ground state and low-lying excited states of the system.

Several prior works studied the quantum circuit implementation of the unitary linear transformation of basis set. The unitary coupled cluster (UCC) method [41–45], particularly with single excitation operators, is widely used as parameterized ansatz circuits for wavefunctions. UCC is achieved by employing an operator $e^{\hat{T}}$, where $\hat{T}$ is anti-Hermitian and represented as $\sum_{i<j} t_{ij}(\boldsymbol{a}_i^\dagger \boldsymbol{a}_j - \boldsymbol{a}_j^\dagger \boldsymbol{a}_i)$. Trotter splitting is then adopted to approximate the operator by a quantum circuit [46–49]. While this UCC quantum circuit is not designed for unitary basis transformation, it could be used as a unitary transformation of the basis set, which is mathematically guaranteed by Thouless theorem [50]. Some other methods are pro-

* *jianfeng@math.duke.edu; *yingzhouli@fudan.edu.cn

posed when they consider preparing the Slater determinant state by rotating the basis set. Wecker *et al.* [10] describe a procedure in which they use a quantum circuit to take unitary transformation of a basis set and prepare arbitrary Slater determinant state. Their circuit has no more than n^2 gates with arbitrary connectivity for n being the size of the basis set. Babbush *et al.* [12] suggest employing the fermionic fast Fourier transform to prepare a Slater determinant state in a plane wave basis. This approach involves rotating the system from a plane wave dual basis, achieving a depth of $O(n)$ while adhering to the planar lattice connectivity constraints found in some existing superconducting quantum platforms [12]. The plane wave dual basis serves as a smooth approximation to a grid structure, which has been explored to enhance the efficiency of density functional calculations [51, 52]. In [11], an efficient strategy is proposed to conduct the unitary linear transformation on a quantum computer with linearly connected qubits, and achieves a gate depth $\frac{n}{2}$, where the gate depth is counted as the number of sequential Givens rotations. The strategy is a variant of the QR decomposition based method of constructing single-particle unitary transformations [10, 53, 54]. Kivlichan *et al.* [11] organize the Givens rotations in QR decomposition in a particular ordering to benefit from the parallelization on linearly connected quantum computer and eliminates redundant rotations based on the symmetry of the Hamiltonian. Some of these unitary linear transformation methods [11, 12] target the quantum circuit implementations of initial state preparations.

Non-unitary linear transformations of basis sets also play an important role in quantum physics and chemistry for both ground state and excited state computations. In ground state computations, for example, Jiménez-Hoyos *et al.* [55] use the non-unitary Thouless theorem [50] to rotate a orthogonal basis Hartree-Fock state to a non-orthogonal basis Hartree-Fock state. Jiménez-Hoyos *et al.* [55] derive the formulas of the Hamiltonian matrix elements of this non-orthogonal Hartree-Fock state. In the excited state computation, if different basis sets (either different basis sets or different transformations of a basis set) are adopted for the ground state and low-lying excited states, calculating the overlap between different states involves a non-unitary linear transformation of basis set. Such a state-specific rotation method for excited state computation could be viewed as a multi-reference (MR) method [56, 57]. Several studies have shown that the integration of state-specific methods with CASSCF can yield higher accuracy, even with a reduced active space [58–61]. Such an approach is referred to as the state-specific CASSCF (SS-CASSCF). SS-CASSCF employs different reference states to generate configuration interaction (CI) functions and incorporates an appropriate orthogonal penalty into the objective function. The computation of this orthogonal penalty requires computing the inner product between two states under different bases. Computing such inner products for certain special cases, *e.g.* Hartree-Fock states or sparse states, has been explored and performed efficiently on classical computers [56, 57, 62–66]. However, in general, if the states exhibit dense configurations, the calculation of such inner products scales exponentially with respect to the basis set size on classical computers.

In this work, we propose a quantum circuit that performs the exact non-unitary linear transformation of a basis set. The gate complexity of the proposed quantum circuit scales polynomially in the basis set size, more specifically scales quadratically in the basis set size, i.e., $O(n^2)$ for n being the basis set size. The circuit depth scales linearly in the basis set size. Combined with regular inner product quantum circuit, we could evaluate the inner product of two states under different basis sets with $O(n^2)$ gates and $O(n)$ depth on a quantum computer. Our major contributions are summarized as follows.

1. We rewrite the unitary linear transformation of basis set using wedge exterior notation, which can then be easily extended to the non-unitary case.

2. A quantum circuit is proposed for non-unitary linear transformations of basis sets. The 1 and 0 singular values of the overlapping matrix between two basis sets are further compressed to reduce the gate complexity.

3. Quantum circuits are proposed to evaluate the inner product of two states in different basis sets.

The remainder of the paper is organized as follows. In the *Results* section, we present our main findings, including the quantum circuit for non-unitary linear transformations of basis sets and the quantum circuit for computing the inner product of two states under different basis sets, as described in Section II A and Section II B respectively. The *Discussion* section concludes the paper and outlines potential directions for future work. In the *Methods* section, we provide detailed derivations and analyses of the proposed quantum circuits. In particular, we review the quantum circuit for unitary linear transformations [11] and reformulate the derivation of the unitary transformation operator in the framework of exterior algebra in Section IV A. Section IV B introduces our novel quantum circuit for non-unitary linear transformations of basis sets, along with analyses of the corresponding gate complexity and circuit depth. Building on this construction, we propose quantum circuits with depth $O(n)$ for evaluating the inner product of two states under different basis sets in Section IV C.

RESULTS

A. Non-Unitary Linear Transformation of Basis Sets

Through mathematical derivation, we show that the linear transformation of basis sets is equivalent to $\wedge\mathbf{u}$

in exterior algebra. Furthermore, we propose a quantum circuit to realize non-unitary linear transformations of basis sets under the setting of Jordan–Wigner transformation [8]. The quantum circuit for the $\wedge \boldsymbol{u}$ can be approximately implemented as follows.

1. Calculate the SVD of u, i.e., $u_{ij} = \sum_{k=1}^{n} \sigma_k L_{ik} R_{kj}$, with singular values σ_is in non-increasing ordering.

2. Round up large singular values of u and truncate small singular values of u, i.e.,

$$\tilde{\sigma}_i = \begin{cases} 1 & \sigma_i \geq 1-\varepsilon \\ \sigma_i & \varepsilon < \sigma_i < 1-\varepsilon \\ 0 & \sigma_i \leq \varepsilon \end{cases}.$$

   Let the number of $\tilde{\sigma}_i = 1$ be s and the rank after truncation be r.

3. Prepare $r-s+1$ ancilla qubits to state $|0\rangle$, denote them as $a_{s+1}, a_{s+1}, \ldots, a_{r+1}$.

4. Apply the unitary operator $J_\psi U(R;\psi) J_\psi^{-1}$ to the n working qubits following the circuit construction in Section IV A.

5. Apply controlled-RY gates controlling from q_i targeting a_i for $i = s+1, \ldots, r$.

6. Apply an X gate to flip ancilla qubit a_{r+1} and then apply a multi-open-controlled Toffoli gate controlling from $q_{r+1}, \ldots, q_n$ targeting a_{r+1}.

7. Apply the unitary operator $J_\psi U(L;\psi) J_\psi^{-1}$ to the n working qubits following the circuit construction in Section IV A.

8. Project all ancilla qubits to $|0\rangle$ state via measurement and post-selection.

The error of the above approximation can be controlled by the threshold ε. The total depth of the quantum circuit is $O(n)$ and the total number of qubits is $n+r-s+1$. All details of the derivations and analysis such as the error bound, gate complexity, and circuit depth as well as the success probability of the post-selection are provided in Section IV A and Section IV B.

Remark. If we remove step 8 and stop at step 7, we actually obtain the quantum circuit corresponding to the block encoding of $\wedge \boldsymbol{u}$. Block-encoding is a standard framework used to embed non-unitary matrices into unitary matrices, allowing them to be implemented as quantum circuits along with some measurements [67]. We will use the block-encoding we provided here in the context of calculating inner products.

In Fig. 1, we provide the quantum circuit for a non-unitary matrix u of dimension 8. After the rounding-up and truncating, the approximated non-unitary matrix has 2 singular values equal to 1 and of rank 5.

B. Quantum Circuit for Inner Product of Two States under Different Basis Sets

We propose a quantum circuit for evaluating the inner product of two states under different basis sets. The quantum circuit is constructed based on the non-unitary linear transformation proposed in Section II A.

For two states $|\Phi\rangle$ and $|\Psi\rangle$ defined with respect to two basis sets $\{|\phi_i\rangle\}_{i=1}^n$ and $\{|\psi_i\rangle\}_{i=1}^n$, and their corresponding qubit representations $|\Phi\rangle_q$ and $|\Psi\rangle_q$, we denote by $\Xi(\psi,\phi)$ the non-unitary linear transformation $\wedge \mathbf{u}$, where $u_{ij} = \langle \psi_i | \phi_j \rangle$. Let $\tilde{\Xi}(\psi,\phi)$ denote the block-encoding of $\Xi(\psi,\phi)$. Under these notations, the inner product $\langle \Phi | \Psi \rangle$ can be evaluated by the following quantum circuits.

Fig. 2 shows the swap test based quantum circuits for evaluating the inner product. This circuit is little different from the original swap test, as we reduce the number of ancilla qubits but increase the number of qubits to be measured. Fig. 3 shows the Hadamard test based quantum circuit for evaluating the inner product. All details of the derivations are provided in Section IV C.

DISCUSSION

In this work, we have proposed a quantum circuit framework for implementing non-unitary basis transformations, which extends beyond the conventional unitary approaches widely used in quantum algorithms. By leveraging the SVD structure of the transformation, our design achieves linear circuit depth with a modest number of ancilla qubits, while maintaining controlled approximation errors. This efficiency makes it feasible to apply basis optimization strategies directly within variational algorithms, such as VQE, and thus to evaluate overlaps of many-body states prepared in different orbital bases. Importantly, this capability enables state-specific treatments, including orbital-optimized excited-state methods such as CASSCF or OptOrbFCI, on quantum platforms. Compared with existing unitary-only schemes, the present framework significantly broadens the scope of quantum simulations by accommodating transformations that are not naturally unitary, thereby opening a path toward more accurate and flexible quantum chemical calculations.

METHODS

A. Unitary Linear Transformation under Exterior Algebra

We review the quantum circuit for unitary linear transformation proposed by Kivlichan *et al.* [11] and rewrite the derivation using exterior algebra in this section.

The unitary linear transformation of basis set discussed

ARTICLE IN PRESS

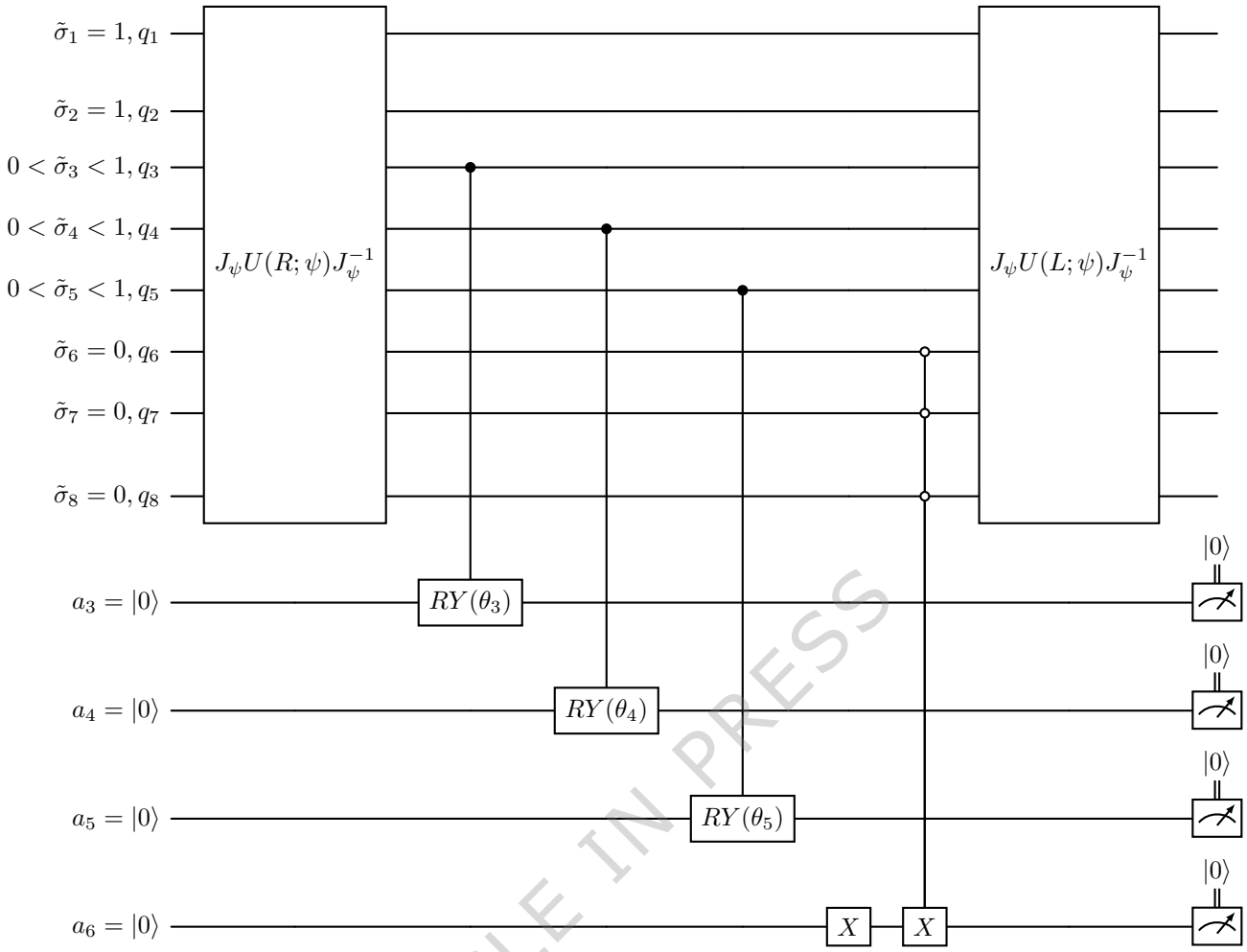


FIG. 1: An example for a nonunitary matrix u of dimension 8 with approximated singular values $\tilde{\sigma}_1 = \tilde{\sigma}_2 = 1$, $1 > \tilde{\sigma}_3 \geq \tilde{\sigma}_4 \geq \tilde{\sigma}_5 > 0$, and $\tilde{\sigma}_6 = \tilde{\sigma}_7 = \tilde{\sigma}_8 = 0$. This quantum circuit is the approximated block encoding of $\wedge \boldsymbol{u}$.

ARTICLE IN PRESS

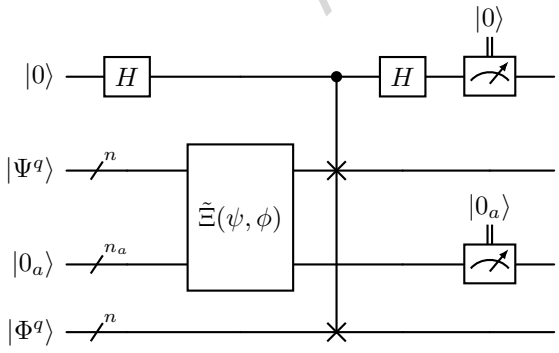


FIG. 2: Swap test circuit to calculate the inner-product $|\langle\Phi|\Psi\rangle|$. The absolute value square $|\langle\Phi|\Psi\rangle|^2$ is the probability of all the measurement being $|0\rangle$.

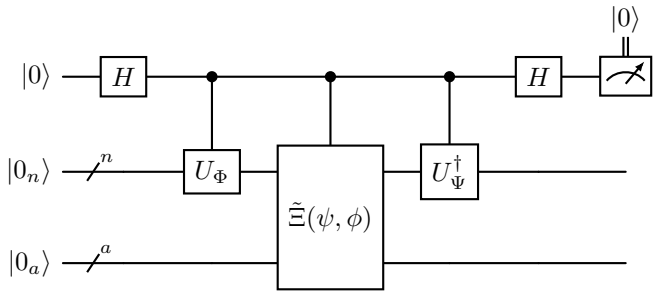


FIG. 3: Hadamard test circuit to calculate $\mathrm{Re}\,\langle\Psi|\Phi\rangle$, which could be inferred from the probabilities of the measurement result.

in [11] admits,

$$|\phi_p\rangle = \sum_{q=1}^{n} |\psi_q\rangle\, u_{qp} \tag{1}$$

where u is an $n \times n$ unitary matrix, $\{|\psi_i\rangle\}_{i=1}^n$ and $\{|\phi_i\rangle\}_{i=1}^n$ are the original and rotated orthonormal basis (spin-orbitals) respectively, and n denotes the basis set size. The associated creation and annihilation operators admit a similar transformation relationship,

$$\boldsymbol{a}^\dagger(\phi_p) = \sum_{q=1}^{n} \boldsymbol{a}^\dagger(\psi_q) u_{qp} \text{ and } \quad \boldsymbol{a}(\phi_p) = \sum_{q=1}^{n} \boldsymbol{a}(\psi_q)(u_{qp})^*,$$

where $\boldsymbol{a}^\dagger(\cdot)$ and $\boldsymbol{a}(\cdot)$ are the creation and annihilation operators associated with the given basis, and $(u_{qp})^*$ is the complex conjugate of u_{qp}.

Given the two one-body basis sets, $\{|\psi_i\rangle\}_{i=1}^n$ and $\{|\phi_i\rangle\}_{i=1}^n$, we could generate two many-body basis sets to represent the many-body states. For two one-body basis sets that are related to each other by a unitary linear transformation, as in (1), their associated many-body basis sets are also related to each other by a unitary linear transformation. The unitary linear transformation in many-body space is characterized by the Thouless theorem [50], which is equivalent to applying the operator,

$$U(u;\psi) = \exp\left(\sum_{p,q=1}^{n} (\log u)_{pq} \boldsymbol{a}^\dagger(\psi_p)\boldsymbol{a}(\psi_q) \right) \tag{2}$$

to the many-body states, where $(\log u)_{pq}$ denotes the (p,q) element of the matrix $\log u$. The notation ψ in $U(u;\psi)$ denotes that all creation and annihilation operators correspond to the basis set $\{|\psi_i\rangle\}_{i=1}^n$.

Now we give a definition of this $U(u;\psi)$ in the language of exterior algebra. Given an n dimensional Hilbert space V with $\{|\psi_i\rangle\}_{i=1}^n$ being its orthonormal basis set, the k-th exterior powers is denoted as $\wedge^k V$. A basis set of $\wedge^k V$ admits,

$$\{|\psi_{i_1}\rangle \wedge \cdots \wedge |\psi_{i_k}\rangle \mid 1 \le i_1 < \cdots < i_k \le n\}. \tag{3}$$

The bases in (3) are orthonormal. For the electronic many-body Schrödinger equation, the k-particle states live in $\wedge^k V$. The exterior algebra of V is defined as, $\wedge V = \oplus_{k\ge 0} \wedge^k V$. An orthonormal basis set of $\wedge V$ admits,

$$\{|\psi_{i_1}\rangle \wedge \cdots \wedge |\psi_{i_k}\rangle \mid 1 \le i_1 < \cdots < i_k \le n \text{ and } k \ge 0\}. \tag{4}$$

The space $\wedge V$ is also known as the Fock space in physics and chemistry. In the following Definition 1, we extend a linear map $\boldsymbol{u} : V \to V$ to a linear map $\wedge\boldsymbol{u} : \wedge V \to \wedge V$.

Definition 1. Let $\boldsymbol{u} : V \to V$ be a linear map. Define $\wedge\boldsymbol{u} : \wedge V \to \wedge V$ as,

$$\wedge\boldsymbol{u}(|\psi_{i_1}\rangle \wedge |\psi_{i_2}\rangle \wedge \cdots \wedge |\psi_{i_k}\rangle) = \boldsymbol{u}\,|\psi_{i_1}\rangle \wedge \boldsymbol{u}\,|\psi_{i_2}\rangle \wedge \cdots \wedge \boldsymbol{u}\,|\psi_{i_k}\rangle,$$

for $1 \le i_1 < \cdots < i_k \le n$ and $k \ge 0$. The linear map $\wedge\boldsymbol{u}$ is called the wedged map of $\boldsymbol{u}$.

When the linear map $\boldsymbol{u}$ is of form,

$$\boldsymbol{u} = \sum_{i,j=1}^{n} u_{ij}\,|\psi_i\rangle\langle\psi_j|, \tag{5}$$

the linear operator $U(u;\psi)$ as in (2) is consistent with $\wedge\boldsymbol{u}$, i.e.,

$$U(u;\psi) = \wedge\boldsymbol{u}.$$

The detailed derivation are provided in the *Supplementary Material*. The derivation gives a proof of Thouless theorem using the language of exterior algebra, which is different from the BCH formula used in Kivlichan *et al.* [11]. We find that the extending linear map $\wedge\boldsymbol{u}$ to non-unitary transformation is straightforward, whereas extending the operator $U(u;\psi)$ to non-unitary case is more difficult. Hence, the linear map $\wedge\boldsymbol{u}$ in exterior algebra will be used throughout the rest paper mainly for non-unitary transformations.

An important property of $U(u;\psi)$ is the operator composition property, which builds the foundation for [11]. Precisely, for any two unitary matrices u^1 and u^2, the composition of $U(u^1;\psi)$ and $U(u^2;\psi)$ is the operator of product of two matrices, i.e.,

$$U(u^1;\psi)U(u^2;\psi) = U(u^1u^2;\psi). \tag{6}$$

Lemma 1 gives an analog composition property for wedged maps.

Lemma 1. Suppose $\boldsymbol{u}^1$ and $\boldsymbol{u}^2$ are two linear maps $V \to V$, then the composition property holds for wedged maps,

$$(\wedge\boldsymbol{u}^1)(\wedge\boldsymbol{u}^2) = \wedge(\boldsymbol{u}^1\boldsymbol{u}^2).$$

We emphasize that two linear maps $\boldsymbol{u}^1$ and $\boldsymbol{u}^2$ in Lemma 1 are not necessary unitary. Lemma 1 holds for non-unitary linear maps as well.

Specifically, we consider two unitary maps defined as,

$$\boldsymbol{u}^1 = \sum_{i,j=1}^{n} u^1_{ij}\,|\psi_i\rangle\langle\psi_j|, \quad \boldsymbol{u}^2 = \sum_{i,j=1}^{n} u^2_{ij}\,|\psi_i\rangle\langle\psi_j|.$$

By the equivalence between $U(u;\psi)$ and $\wedge\boldsymbol{u}$, we have $U(u^1;\psi) = \wedge\boldsymbol{u}^1$ and $U(u^2;\psi) = \wedge\boldsymbol{u}^2$. Therefore, the composition of two operators admits,

$$U(u^1u^2;\psi) = U(u^1;\psi)U(u^2;\psi) = (\wedge\boldsymbol{u}^1)(\wedge\boldsymbol{u}^2) = \wedge(\boldsymbol{u}^1\boldsymbol{u}^2).$$

Such a composition property agrees with the composition of maps $\boldsymbol{u}^1$ and $\boldsymbol{u}^2$,

$$\boldsymbol{u}^1\boldsymbol{u}^2 = \sum_{i,j=1}^{n} (u^1u^2)_{ij}\,|\psi_i\rangle\langle\psi_j|,$$

where u^1u^2 denotes the product of two matrices.

Next, we discuss the quantum circuit implementation of $U(u;\psi)$. For general unitary operator in exponent

ARTICLE IN PRESS

form, e.g., (2), Trotterization is widely adopted in quantum computing, especially in quantum simulation [8, 68]. The Trotterization leads to many number of small time steps and accumulation of truncation errors. For the particular unitary operator $U(u;\psi)$ as in (2), Kivlichan *et al.* [11] proposes a tailored quantum circuit based on Givens QR factorization of u. In the original work [11], real orthogonal matrix u are considered in detail, and an expression for complex unitary u is provided without detail. In this paper, we revisit and rederive the decomposition for complex unitary matrix u directly. Notably, the final expression is slightly different from that in [11], which should be due to typos therein.

The complex Givens rotation is composed of three parts: two phase rotations and a regular real Givens rotation. The phase rotation acting on the q-th row of a matrix with rotation angle ϕ is denoted as $p_q(\phi) = \mathrm{Diag}\{1,\ldots,1,e^{-\imath\phi},1\ldots,1\}$, i.e., the identity matrix except the p-th 1 replaced by $e^{-\imath\phi}$. The regular real Givens rotation by an angle θ between the p-th and q-th rows of a matrix is denoted as $r_{pq}(\theta_{pq})$. Contrast to the regular real Givens rotation, the complex Givens rotation first multiplies the elements to be eliminated by complex signs, i.e., phase rotations, to make them real, and then performs the real Givens rotation. For example, let us consider the case using u_{pi} to eliminate u_{qi}, where both u_{pi} and u_{qi} are complex numbers. The phase rotations, $p_p(\phi_p)$ and $p_q(\phi_q)$, are chosen such that $e^{-\imath\phi_p}u_{pi} = |u_{pi}|$ and $e^{-\imath\phi_q}u_{qi} = |u_{qi}|$, respectively. Then the real Givens rotation, $r_{pq}(\theta_{pq})$, is constructed with,

$$\theta_{pq} = \arccos\frac{|u_{pi}|}{\sqrt{|u_{pi}|^2+|u_{qi}|^2}}.$$

By these constructions, after we multiply $g_{pq} = r_{pq}(\theta_{pq})p_q(\phi_q)p_p(\phi_p)$ to u, the (q,i) entry is zeroed out. Using the complex Givens rotation and regular Givens QR factorization procedure, a unitary matrix u is decomposed as,

$$u = \prod_{pq} g^*_{pq} \cdot \prod_{i=1}^{n} p^*_i(\phi_i), \tag{7}$$

where

$$\begin{aligned} g^*_{pq} &= p_p(-\phi_p)p_q(-\phi_q)r_{pq}(-\theta_{pq}), \text{ and}\\ p^*_i &= p_i(-\phi_i). \end{aligned}$$

Notice that there are $\frac{n(n-1)}{2}$ complex Givens rotations in the first product of (7), and the ordering of $\{pq\}$ pairs is not unique. Kivlichan *et al.* [11] propose a specific ordering of $\{pq\}$ to maximize the parallelizability in applying these complex Givens rotations on quantum computer.

By the definition of $U(u;\psi)$, we could define the operation of $U(r_{pq};\psi)$ and $U(p_p;\psi)$, and denote them, respectively, as

$$\boldsymbol{R}_{pq}(\theta;\psi) = U(r_{pq}(\theta);\psi), \text{ and} \tag{8}$$
$$\boldsymbol{P}_p(\phi;\psi) = U(p_p(\phi);\psi). \tag{9}$$

The corresponding "complex Givens rotation" and its adjoint admit,

$$\begin{aligned} \boldsymbol{G}_{pq} &= U(g_{pq}) = \boldsymbol{R}_{pq}(\theta_{pq})\boldsymbol{P}_q(\phi_q)\boldsymbol{P}_p(\phi_p), \text{ and}\\ \boldsymbol{G}^*_{pq} &= U(g^*_{pq}) = \boldsymbol{P}_p(-\phi_p)\boldsymbol{P}_q(-\phi_q)\boldsymbol{R}_{pq}(-\theta_{pq}), \end{aligned} \tag{10}$$

where we omit ψ, and some θ_{pq}, ϕ_p, ϕ_q for simplicity. Under these notations, the operation $U(u;\psi)$ could be decomposed into many operations of $\boldsymbol{G}_{pq}$ and $\boldsymbol{P}_i$ for u defined in (7),

$$U(u;\psi) = \prod_{pq}\boldsymbol{G}^*_{pq}\prod_{i=1}^{n}\boldsymbol{P}^*_i(\phi_i;\psi). \tag{11}$$

Next we demonstrate that the decomposition (11) is sufficiently simple and could be implemented using quantum gates directly. By (2), the explicit expressions of $\boldsymbol{P}_p = U(p_p(\phi);\psi)$ and $\boldsymbol{R}_{pq} = U(r_{pq}(\theta);\psi)$ could be written as

$$\boldsymbol{P}_p(\phi;\psi) = \exp(-\imath\phi_p\boldsymbol{n}(\psi_p)), \text{ and} \tag{12}$$
$$\boldsymbol{R}_{pq}(\theta;\psi) = \exp\left[\theta_{pq}(\boldsymbol{a}^\dagger(\psi_p)\boldsymbol{a}(\psi_q) - \boldsymbol{a}^\dagger(\psi_q)\boldsymbol{a}(\psi_p))\right], \tag{13}$$

where the detailed derivations could be found in the *Supplementary Material*.

Now, we turn to the quantum circuit designs for $U(u;\psi)$. To make our discussion rigorous, we make a strict distinction between the quantum state of the physical system being studied and the qubit state in the encoded space of a quantum computer. They are linked to each other by encoded mappings. Here the mapping is the Jordan–Wigner transformation as in Definition 2.

Definition 2. The Jordan–Wigner transformation of basis $\{|f_i\rangle \mid i = 1,2,\ldots,n\}$ is denoted as J_f, such that:

$$J_f(|f_{i_1}\rangle \wedge |f_{i_2}\rangle \wedge \cdots \wedge |f_{i_k}\rangle) = |n_1n_2n_3\cdots\rangle,$$

where $n_1n_2n_3\cdots$ is a bit string of length equals to the size of basis set n. And $n_i = 1$ if $i \in \{i_1,i_2,\ldots,i_k\}$, $n_i = 0$ otherwise.

These basis vectors $\{|f_i\rangle \mid i = 1,2,\ldots,n\}$ do not need to be a physically meaningful basis, they can be arbitrary abstract basis of any abstract vector space, such as $|f_i\rangle$ is the i-th unit coordinate vector of $\mathbb{C}^n$. By this definition, the creation and annihilation operators under Jordan–Wigner transformation are the same as the usual definition, i.e.,

$$\begin{aligned} \boldsymbol{a}^\dagger_i &= J_f\boldsymbol{a}^\dagger(f_i)J_f^{-1}\\ &= Z_1\otimes\cdots\otimes Z_{i-1}\otimes(|1\rangle\langle 0|)\otimes I_{i+1}\otimes\cdots\otimes I_n, \text{ and}\\ \boldsymbol{a}_i &= J_f\boldsymbol{a}(f_i)J_f^{-1}\\ &= Z_1\otimes\cdots\otimes Z_{i-1}\otimes(|0\rangle\langle 1|)\otimes I_{i+1}\otimes\cdots\otimes I_n. \end{aligned} \tag{14}$$

Both ket-bra operations, $|1\rangle\langle 0|$ and $|0\rangle\langle 1|$, are applied to the index i qubit in the above definitions. There is no

ARTICLE IN PRESS

basis notation in $\boldsymbol{a}_i^\dagger$ and $\boldsymbol{a}_i$ because they are operators on qubit states. Basis information are kept in the encoding mapping J_f. This viewpoint is helpful in the section of inner-product of two states under different bases in Section IV C.

$$\begin{pmatrix} * & * & * & * & * \\ 4 & * & * & * & * \\ 3 & 5 & * & * & * \\ 2 & 4 & 6 & * & * \\ 1 & 3 & 5 & 7 & * \end{pmatrix} \tag{15}$$

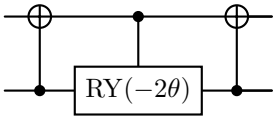
Now, we turn to the quantum circuit design for $U(u;\psi)$. To maximize parallelism on a quantum computer with linearly connected qubits, Kivlichan *et al.* [11] proposed a specific elimination order for the complex Givens rotations. An example for $n = 5$ is shown in Eq. (15). In this elimination order, the lower-triangular elements of a 5×5 unitary matrix are sequentially removed using complex Givens rotations. Each non-asterisk entry indicates an off-diagonal element to be eliminated, with the number specifying the step at which its upper neighbor removes it. Entries with the same number can be zeroed out in parallel. Asterisks (*) mark entries on or above the main diagonal, which do not require explicit elimination. Once all elements below the diagonal are removed, the matrix becomes diagonal automatically. During this procedure, complex Givens rotations are consistently applied to neighboring rows, ensuring that the Z-strings introduced by the Jordan—Wigner transformation cancel out. This elimination strategy enhances parallelizability, allowing, in the best case, $O(n)$ elements to be eliminated simultaneously. Consequently, using this specific elimination order results in a quantum circuit of depth $O(n)$.

We provide an observation that further simplifies the expression of $U(u;\psi)$. After Givens QR upper triangularization, the resulting diagonal matrix typically has all elements equal to 1 except the last bottom-right element. This is due to the phase rotations and unitarity of u. Hence, the $U(u;\psi)$ expression (11) could be rephrased as

$$U(u;\psi) = \prod_i \left[\prod_{q \in \mathrm{Step}_i} (\boldsymbol{G}^{(i)}_{q-1,q})^* \right] \cdot \boldsymbol{P}_n^*(\phi_n;\psi). \tag{16}$$

The upper index i of the gate $\boldsymbol{G}^{(i)}_{q-1,q}$ denotes the i-th step of parallel complex Givens rotations and the set Step_i is the row indices of the elements eliminated in parallel at the i-th step. Comparing to (11), the product of phase operators is simplified by a single phase operator acting on the n-th row, and parallel sequence of the gates is also indicated.

The quantum circuit for $U(u;\psi)$ can be obtained by composing some basic quantum gates. If we denote the first line as the qubit $q-1$ and the second as the qubit q, we have

$$J_\psi \boldsymbol{R}_{q-1,q}(\theta;\psi) J_\psi^{-1} =$$ 

, (17)

where J_ψ is the Jordan–Wigner transformation defined as Definition 2. Similarly, for the phase operator, it is just a single qubit gate acting on the p-th qubit as in (18) below.

$$J_\psi \boldsymbol{P}_p(\phi;\psi) J_\psi^{-1} = \boxed{\begin{pmatrix} 1 & 0 \\ 0 & e^{-\imath\phi} \end{pmatrix}}. \tag{18}$$

All the details of the derivations of these two quantum circuits are given in the *Supplementary Material*.

Then combining the rotation quantum circuit as in (17) together with that of the phase gate in (18), we obtain the quantum circuit for complex Givens rotations applied to adjacent rows, which is denoted as $\boldsymbol{G}^{(i)}_{q-1,q}$. The overall quantum circuit for $J_\psi U(u;\psi) J_\psi^{-1}$ corresponding to a 5×5 unitary map $\boldsymbol{u}$ is given in Fig. 4. The parallel steps are consistent with that in Eq. (15).

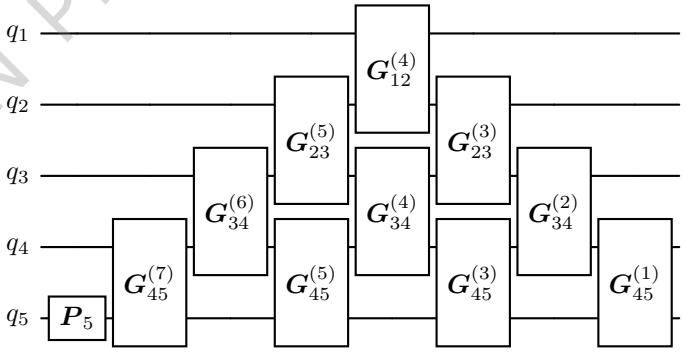


FIG. 4: Quantum circuit for $J_\psi U(u;\psi) J_\psi^{-1}$. All gates are their complex conjugates.

Remark. Comparing to the original work [11], we extend the discussion to complex unitary matrix in detail and provide the corresponding quantum circuit. At the same time, we rewrite some expressions using the exterior algebra notations, which serves as an introduction of notations for our later sections.

B. Non-Unitary Linear Transformation by SVD

We naturally raise a question: when u is non-unitary, can we extend the linear transformation in Section IV A? The answer is yes, but the derivation is more complicated and the resulting quantum circuit is about twice the depth of the unitary one. There are at least two potential applications for the non-unitary linear transformation: a) calculating the overlap between two states

ARTICLE IN PRESS

under different bases, which is detailed in the next section; b) change of basis to a non-orthogonal one.

As we mentioned earlier, the Thouless theorem in (2) form is too difficult to be extended to non-unitary case, which is mainly due to the logarithm of a non-unitary matrix. Hence, we stick to exterior algebra representation of Thouless theorem and all later derivations are in the language of exterior algebra. We recall the notation we use, i.e., $U(u;\psi)$ and $\wedge\boldsymbol{u}$. When u is a unitary matrix, two operators are equal $U(u;\psi) = \wedge\boldsymbol{u}$, for $U(u;\psi)$, $\wedge\boldsymbol{u}$ and $\boldsymbol{u}$ being defined in (2), Definition 1, and (5), respectively. When u is non-unitary, we use $\wedge\boldsymbol{u}$ for the linear map and avoid using $U(u;\psi)$.

In order to reduce the overall circuit depth for the non-unitary linear transformation, our construction relies on the singular value decomposition (SVD) of u and hence its operator $\boldsymbol{u}$. Without loss of generality, we assume that the u is a square matrix. If not, we can always pad the rectangular matrix with zeros to make it square. Thus we will restrict our discussion to the square matrix case. At the end of this section, we will briefly discuss how to estimate the cost of resources for general rectangular cases.

Let the SVD of a non-unitary matrix u be of form,

$$u = LDR,$$

where L and R are left and right singular vectors, $D = \mathrm{diag}(\sigma_1, \ldots, \sigma_n)$ is a diagonal matrix with singular values in non-increasing ordering, i.e., $\sigma_1 \geq \cdots \geq \sigma_n$. We further assume that u is a nonunitary matrix with 2-norm bounded by one, i.e., $1 \geq \sigma_1 \geq \cdots \geq \sigma_n$. Singular vectors L and R are unitary matrices. Let $\{|\psi_i\rangle\}_{i=1}^n$ be the set of underlying basis set. The operator $\boldsymbol{u}$ associated with u also admits an operator SVD,

$$\boldsymbol{u} = \boldsymbol{LDR}, \tag{19}$$

where $\boldsymbol{L}$, $\boldsymbol{D}$, and $\boldsymbol{R}$ are associated with matrices L, D, and R respectively,

$$\begin{aligned}
\boldsymbol{L} &= \sum_{i,j=1}^{n} L_{ij} \left|\psi_i\right\rangle \left\langle\psi_j\right|, \\
\boldsymbol{D} &= \sum_{i=1}^{n} \sigma_i \left|\psi_i\right\rangle \left\langle\psi_i\right|, \text{ and} \\
\boldsymbol{R} &= \sum_{i,j=1}^{n} R_{ij} \left|\psi_i\right\rangle \left\langle\psi_j\right|.
\end{aligned}$$

By Lemma 1, we have $\wedge\boldsymbol{u} = (\wedge\boldsymbol{L})(\wedge\boldsymbol{D})(\wedge\boldsymbol{R})$. For unitary matrices L and R, the operators $\wedge\boldsymbol{L} = U(L;\psi)$ and $\wedge\boldsymbol{R} = U(R;\psi)$ can be implemented by quantum circuits as in Section IV A, e.g., analog quantum circuits of Fig. 4. In the following, we focus on the quantum circuit construction for the wedged diagonal operator $\wedge\boldsymbol{D}$.

We first rewrite $\wedge\boldsymbol{D}$ as a composition of at most n simple operators, which are simple to be implemented by quantum gates. According to Definition 1, the action of $\wedge\boldsymbol{D}$ on an exterior algebra is defined as applying the operator $\boldsymbol{D}$ to all one-body states, as,

$$\begin{aligned}
&(\wedge\boldsymbol{D}) \left|\psi_{i_1}\right\rangle \wedge \left|\psi_{i_2}\right\rangle \wedge \cdots \wedge \left|\psi_{i_k}\right\rangle \\
&= \boldsymbol{D} \left|\psi_{i_1}\right\rangle \wedge \boldsymbol{D} \left|\psi_{i_2}\right\rangle \wedge \cdots \wedge \boldsymbol{D} \left|\psi_{i_k}\right\rangle \\
&= \sigma_{i_1}\sigma_{i_2}\cdots\sigma_{i_k} \left|\psi_{i_1}\right\rangle \wedge \left|\psi_{i_2}\right\rangle \wedge \cdots \wedge \left|\psi_{i_k}\right\rangle.
\end{aligned} \tag{20}$$

It is worth noting that this expression is closely related to the particle number operator. It acts like a weighted number operator. More explicitly, if the many-body state includes the state $|\psi_i\rangle$, the result of the operation will give a factor σ_i. Thus, we define an operator

$$\boldsymbol{\nu}(\psi_j) = \mathbf{1} + (\sigma_j - 1)\boldsymbol{n}(\psi_j),$$

which admits,

$$\begin{aligned}
&\boldsymbol{\nu}(\psi_j)(\left|\psi_{i_1}\right\rangle \wedge \left|\psi_{i_2}\right\rangle \wedge \cdots \wedge \left|\psi_{i_k}\right\rangle) \\
&= \begin{cases} \sigma_j(\left|\psi_{i_1}\right\rangle \wedge \left|\psi_{i_2}\right\rangle \wedge \cdots \wedge \left|\psi_{i_k}\right\rangle), & j \in \{i_1, i_2, \ldots, i_k\} \\ \left|\psi_{i_1}\right\rangle \wedge \left|\psi_{i_2}\right\rangle \wedge \cdots \wedge \left|\psi_{i_k}\right\rangle, & j \notin \{i_1, i_2, \ldots, i_k\} \end{cases}.
\end{aligned}$$

Here $\boldsymbol{n}(\psi_j) = \boldsymbol{a}^\dagger(\psi_j)\boldsymbol{a}(\psi_j)$ is the number operator. Next, we justify that the wedge operator $\wedge\boldsymbol{D}$ is equivalent to the composition of $\boldsymbol{\nu}(\psi_j)$. For any basis $|\psi_{i_1}\rangle \wedge \cdots \wedge |\psi_{i_k}\rangle$ in the exterior algebra (Fock space), the action of the composition of $\boldsymbol{\nu}(\psi_j)$ admits,

$$\begin{aligned}
&\left(\prod_{j=1}^{n} \boldsymbol{\nu}(\psi_j)\right) \left|\psi_{i_1}\right\rangle \wedge \left|\psi_{i_2}\right\rangle \wedge \cdots \wedge \left|\psi_{i_k}\right\rangle \\
&= \sigma_{i_1}\sigma_{i_2}\cdots\sigma_{i_k} \left|\psi_{i_1}\right\rangle \wedge \left|\psi_{i_2}\right\rangle \wedge \cdots \wedge \left|\psi_{i_k}\right\rangle
\end{aligned}$$

which equals (20). Hence, we conclude that the product operator $\prod_{j=1}^{n} \boldsymbol{\nu}(\psi_j)$ is another form of $\wedge\boldsymbol{D}$, i.e.,

$$\wedge\boldsymbol{D} = \prod_{j=1}^{n} \boldsymbol{\nu}(\psi_j).$$

Now we move on to the quantum circuit implementation of composed operator $\wedge\boldsymbol{D} = \prod_{j=1}^{n} \boldsymbol{\nu}(\psi_j)$. Obviously, $\boldsymbol{\nu}(\psi_j)$ is not a unitary operator, and hence, cannot be implemented by quantum circuits directly. We introduce an ancilla qubit to encode the action of $\boldsymbol{\nu}(\psi_j)$. In the context of the Jordan–Wigner transformation, the particle number operator admits,

$$\boldsymbol{n}_j = I_1 \otimes \cdots \otimes I_{j-1} \otimes \begin{pmatrix} 0 & 0 \\ 0 & 1 \end{pmatrix} \otimes I_{j+1} \otimes \cdots \otimes I_n.$$

We define an operator acting on qubit state as $\boldsymbol{\nu}_j$ admitting,

$$\begin{aligned}
\boldsymbol{\nu}_j &= J_\psi \boldsymbol{\nu}(\psi_j) J_\psi^{-1} \\
&= I_1 \otimes \cdots \otimes I_{j-1} \otimes \begin{pmatrix} 1 & 0 \\ 0 & \sigma_j \end{pmatrix} \otimes I_{j+1} \otimes \cdots \otimes I_n,
\end{aligned}$$

where the operator norm is bounded by 1 and so is σ_j.

ARTICLE IN PRESS

We divide the discussion of quantum circuit implementation of $\boldsymbol{\nu}_j$ into three cases: $\sigma_j = 1$, $0 < \sigma_j < 1$, and $\sigma_j = 0$. For simplicity, we drop the subscript j in the following discussion.

When $\sigma = 1$, the corresponding operator $\boldsymbol{\nu}$ is an identity operator, which does not require any quantum gates and any ancilla qubit.

When $0 < \sigma < 1$, the corresponding operator $\boldsymbol{\nu}$ is nonunitary. To incorporate this operation into a quantum circuit, we adopt an extra ancilla qubit. The particular block encoding we use for the 2-by-2 matrix in $\boldsymbol{\nu}$ admits,

$$\tilde{\boldsymbol{\nu}} = \begin{pmatrix} 1 & 0 & 0 & 0 \\ 0 & \sigma & 0 & -\sqrt{1-\sigma^2} \\ 0 & 0 & 1 & 0 \\ 0 & \sqrt{1-\sigma^2} & 0 & \sigma \end{pmatrix} = \begin{pmatrix} 1 & 0 & 0 & 0 \\ 0 & \cos\frac{\theta}{2} & 0 & -\sin\frac{\theta}{2} \\ 0 & 0 & 1 & 0 \\ 0 & \sin\frac{\theta}{2} & 0 & \cos\frac{\theta}{2} \end{pmatrix},$$

where the first qubit is the ancilla qubit and the second one is the working qubit, and $\theta = 2\arccos\sigma$. This encoded matrix $\tilde{\boldsymbol{\nu}}$ on 2-qubit is the controlled-RY gate, denoted as CRY(θ). This controlled-RY gate applies a rotation around the Y-axis by an angle θ to the ancilla qubit and controlled by the working qubit. Denote P_a as the projection operator that project the ancilla qubit to $|0\rangle$ state, which could be implemented via a measurement, then the construction $\tilde{\boldsymbol{\nu}}$ satisfies

$$P_a \tilde{\boldsymbol{\nu}} |0\rangle \otimes |\alpha\rangle = |0\rangle \otimes \boldsymbol{\nu} |\alpha\rangle .$$

The quantum circuit for $\tilde{\boldsymbol{\nu}}$ is given in Fig. 5.

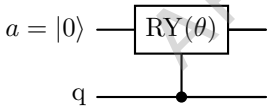


FIG. 5: Quantum circuit of embedded 2-qubit gate. Ancilla qubit is denoted as a, which is initialized to $|0\rangle$ state. The second qubit q is the working qubit which $\boldsymbol{\nu}$ is acted on.

The last case is that $\sigma = 0$. The technique used for $0 < \sigma < 1$ case applies to the $\sigma = 0$ case as well. Then for each $\tilde{\boldsymbol{\nu}}_j$ with singular value $\sigma_j = 0$, we need an ancilla qubit. Instead, we implement the quantum circuit for all $\sigma = 0$ together and use only one ancilla qubit to perform the block encoding.

Let $r = \arg\max_i \{\sigma_i > 0\}$ be the rank of the nonunitary matrix u. Then we have $\sigma_i > 0$ for $i = 1, \ldots, r$ and $\sigma_i = 0$ for $i = r+1, \ldots, n$. Noting that $\boldsymbol{\nu}_j$ with $\sigma_j = 0$ is the projection that projects qubit q_j onto $|0\rangle$ state. Thus, the composition of operators

$$\prod_{i=r+1}^{n} \boldsymbol{\nu}_i$$

is the projection that projects qubits indexed from $r+1$ to n to $|0\cdots0\rangle$. It can be implemented as a X gate combined with a multi-open-controlled Toffoli gate. More specifically, given an ancilla qubit at state $|0\rangle$ and working qubits $q_{r+1}, \ldots, q_n$, we first flip the ancilla qubit to state $|1\rangle$ via an X gate. Then targeting the ancilla qubit, we apply a multi-open-controlled Toffoli gate controlled from all working qubits $q_{r+1}, \ldots, q_n$. Open-controlled gate means that the gate is applied only if the controlling qubits are in state $|0\cdots0\rangle$. After these two gates, the quantum state will be linear combination of

$$|0\rangle |0\cdots0\rangle \quad \text{and} \quad |1\rangle |0\cdots0\rangle_\perp ,$$

where the first qubit is ancilla, the rest are working qubits $q_{r+1}, \ldots, q_n$, and $|0\cdots0\rangle_\perp$ is a state perpendicular to $|0\cdots0\rangle$. Hence, applying a measurement with selected result, i.e., projecting the ancilla qubit to $|0\rangle$, will turn all working qubits $q_{r+1}, \ldots, q_n$ to state $|0\rangle$. Thus, such a quantum circuit is the block encoding as we need. This scheme reduces the number of ancilla qubits down to one for low-rank linear transformations u. However, the actual quantum circuit depth in implementing the multi-open-controlled Toffoli gate depends on the underlying quantum computer hardware, which is beyond the scope of this paper. Figure 6 illustrates the detailed quantum circuit for the case $\sigma = 0$.

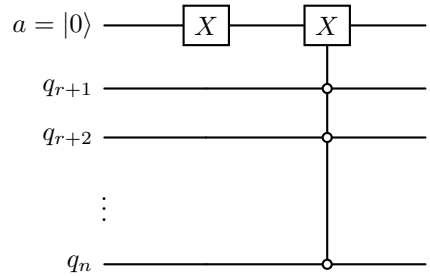


FIG. 6: Block encoding for all $\boldsymbol{\nu}_j$ with $\sigma_j = 0$. Here the ancilla qubit a is initialized to $|0\rangle$ state. Other q_j for $r < j \leq n$ are working qubits corresponding to zero singular values of u.

As discussed above, both cases $\sigma = 1$ and $\sigma = 0$ lead to more quantum resource efficient circuit implementation than that of case $0 < \sigma < 1$. Hence, naturally, we consider rounding up some large singular values to one and truncating some small singular values to zero. Although both rounding up and truncating reduce the quantum resource cost, both of them would introduce approximation errors. Denote the modification on the j-th singular values as ϵ_j. The approximation error introduced by both

ARTICLE IN PRESS

the rounding-up and truncating could be bounded as,

$$\left\| \otimes_{j=1}^{n} \begin{pmatrix} 1 & 0 \\ 0 & \sigma_j + \epsilon_j \end{pmatrix} - \otimes_{j=1}^{n} \begin{pmatrix} 1 & 0 \\ 0 & \sigma_j \end{pmatrix} \right\| \leq \sum_{j=1}^{n} \epsilon_j,$$

where the matrix 2-norm is used. Let $\tilde{u}$ denote the matrix that shares the same singular vectors as u, but has rounded up or truncated singular values, i.e., $\tilde{u}_{ij} = \sum_{k=1}^{n} \tilde{\sigma}_k L_{ik} R_{kj} = \sum_{k=1}^{n} (\sigma_k + \epsilon_k) L_{ik} R_{kj}$. In this context, the error of approximated wedge operator can be bounded more concisely as,

$$\| \wedge \boldsymbol{u} - \wedge \tilde{\boldsymbol{u}} \| \leq \sum_{j=1}^{n} \epsilon_j. \tag{21}$$

Therefore, the overall approximation error could be well-controlled if all ϵ_js are small.

Finally, we assemble all above techniques together and propose the quantum circuit construction of a non-unitary linear transformation $\wedge \boldsymbol{u}$. The overall quantum circuit has been illustrated in Section II A.

Now we briefly discuss success probability for block-encoding. The success probability refers to the likelihood that the block-encoding procedure will successfully prepare the desired quantum state. For an input state $|I\rangle$, the success probability is just the

$$p(|I\rangle) = \| \wedge \boldsymbol{u} \, |I\rangle \|^2,$$

which also equals to the renormalization constant for the transformation. This value mainly depends on the distribution of singular values $\boldsymbol{D}$. Let V be the span of $|\psi_i\rangle_{i=1}^{N}$, i.e., the domain of $\boldsymbol{u}$. For any subspace $W \subseteq V$, we denote the restriction of $\boldsymbol{u}$ to W as $\boldsymbol{u}|_W$. Let P_W be the projector from V onto W, and $P_{\wedge W}$ the projector from $\wedge V$ onto $\wedge W$ defined as $\wedge P_W$. Then, for any input state $|I\rangle \in \wedge V$, the success probability can be lower bounded by

$$p(|I\rangle) \geq \| \wedge (\boldsymbol{u}|_W)(P_{\wedge W} \, |I\rangle) \|^2 \geq \| P_{\wedge W} \, |I\rangle \|^2 \prod_{i \in \mathcal{K}} \sigma_i^2(\wedge W),$$

where $\sigma_i(\wedge W)$ are the singular values of $\boldsymbol{u}|_W$, and $\mathcal{K}$ is the index set of the smallest k singular values, with k being the particle number of $|I\rangle$. Intuitively, the success probability is higher if the input state $|I\rangle$ has a large overlap with the space generated by the intersection of V and and transformation terminal space, and if the corresponding singular values σ are not too small.

We should emphasize that this success probability does not pose any restriction for our protocol in Section IV C, since we do not need to perform further operations conditioned on the post-selected "success" state, we only require application of the whole block-encoding as the Fig. 2 and Fig. 3 illustrate. Further details are provided in Section IV C.

Finally, we present an estimate of the cost of this method. To implement this non-unitary basis transformation, the cost arises from two sources. The first is the classical computational cost, which involves performing an SVD on the non-unitary matrix and Givens QR decompositions of the left and right singular vectors. For a general dense $n \times m$ or $m \times n$ matrix u with $n \geq m$ padded to $n \times n$, one set of singular vectors takes a block-diagonal form, where one block is the usual $m \times m$ singular vectors and the other is an $(n-m) \times (n-m)$ identity matrix. Additionally, the singular values are padded with $n - m$ zeros. The computational cost is thus equivalent to performing a full (non-reduced) SVD on the original rectangular matrix.

The second is the cost of quantum resources. The quantum circuit depth and the number of gates can also be estimated based on the matrix dimension m and n, approximated number of ones s and approximated rank r. The dimension of L and R are both n, with one of them is in the block-diagonal form as mentioned above. And the numbers of gates, as in Section IV A for the unitary case, are bounded by $\frac{n^2+m^2}{2} + O(n+m)$ rotation gates (17) and $n^2 + m^2 + O(n+m)$ phase gates. When qubits are assumed to be linearly connected, the circuit depths for L and R are bounded by $O(n)$ or $O(m)$ times the rotation gate depth. The number of gates for the $\prod_{k=1}^{n} \boldsymbol{\nu}_k$ part depends on the gate counting of the multi-open-controlled Toffoli gate. The quantum circuit for the singular value part costs $r - s + 2$ simple gates and one multi-open-controlled Toffoli gate. The circuit depth is bounded by that of the multi-open-controlled Toffoli gate. Applying the standard decomposition as in [8], an additional ancilla qubit is used, and the quantum circuit depth is $O((n-r)^2)$ for $n - r$ being the number of controlling qubits. Overall, the total quantum circuit depth is bounded by $O((n-r)^2 + n + m)$.

C. Inner Product between States under Different Basis Sets

We consider two sets of one-body bases, $\{|\psi_i\rangle\}_{i=1}^{n}$ and $\{|\phi_j\rangle\}_{j=1}^{n}$. The inner products between all pairs of bases $|\psi_i\rangle$ and $|\phi_j\rangle$ are available and denoted as u_{ij}, i.e., $u_{ij} = \langle \psi_i | \phi_j \rangle$, for $1 \leq i, j \leq n$. For the sake of notation, we assume two bases are of the same dimension n. Our proposed algorithm could be easily extended to two bases of different dimensions. Two many-body states are denoted as $|\Psi\rangle$ and $|\Phi\rangle$, i.e.,

$$|\Psi\rangle = \sum_{1 \leq i_1 < i_2 < \cdots < i_k \leq n} c_{i_1 i_2 \ldots i_k} \, |\psi_{i_1}\rangle \wedge |\psi_{i_2}\rangle \wedge \cdots \wedge |\psi_{i_k}\rangle \,,$$

$$|\Phi\rangle = \sum_{1 \leq i_1 < i_2 < \cdots < i_k \leq n} c'_{i_1 i_2 \ldots i_k} \, |\phi_{i_1}\rangle \wedge |\phi_{i_2}\rangle \wedge \cdots \wedge |\phi_{i_k}\rangle \,.$$

We consider the scenario such that both many-body states are already encoded and prepared in quantum computer, where these states might be generated from ansatz circuits used in VQE framework, from quantum simulations, or initial state preparation methods. The

ARTICLE IN PRESS

encoded many-body states on quantum computer are denoted as,

$$|\Psi^q\rangle = \sum_{I=0}^{2^n-1} d_I\,|I\rangle\,, \quad \text{and } |\Phi^q\rangle = \sum_{I=0}^{2^n-1} d'_I\,|I\rangle\,,$$

where $|I\rangle$ is a bit string representing states on quantum computer. States $|\Psi\rangle$ and $|\Psi^q\rangle$ are connected via a quantum encoding or transformation $\boldsymbol{Q}_\psi$, where the subscript ψ indicates that the encoding is related to basis $\{|\psi_i\rangle\}_{i=1}^n$. Similarly, states $|\Phi\rangle$ and $|\Phi^q\rangle$ are connected via $\boldsymbol{Q}_\phi$. More precisely, the connections admit,

$$\boldsymbol{Q}_\psi\,|\Psi\rangle = |\Psi^q\rangle\,, \quad \text{and } \boldsymbol{Q}_\phi\,|\Phi\rangle = |\Phi^q\rangle\,.$$

When Jordan–Wigner encoding is adopted, $\boldsymbol{Q}_\psi$ is the same as J_ψ. Here, we use $\boldsymbol{Q}_\psi$ as the encoding map to include other encodings, e.g., parity encoding, Bravyi-Kitaev encoding, etc.

When two basis sets are the same and the encoding is also the same and unitary, the inner product between two states $|\Psi\rangle$ and $|\Phi\rangle$ is the same as that of two states on quantum computer, i.e.,

$$\langle\Phi|\Psi\rangle = \langle\Phi^q|\Psi^q\rangle\,.$$

Then, we could use many standard quantum circuits to evaluate it or its modulus. A commonly used one is the swap test as in Fig. 7. Other choices are also widely used in excited state calculations [40, 69]. However, when two states $|\Psi\rangle$ and $|\Phi\rangle$ are under different basis sets, none of the aforementioned quantum circuits for $\langle\Phi^q|\Psi^q\rangle$ can be used directly, due to the fact that $\langle\Phi|\Psi\rangle \neq \langle\Phi^q|\Psi^q\rangle$.

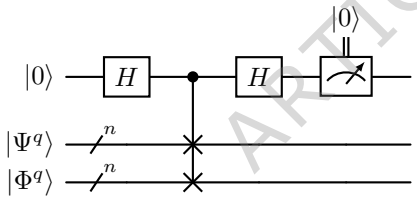


FIG. 7: Swap test circuit to calculate the modulus of the inner-product $|\langle\Phi^q|\Psi^q\rangle|$. The modulus square $|\langle\Phi^q|\Psi^q\rangle|^2$ equals to the probability of the measurement result being $|0\rangle$.

Notice that the inner product of two states is of a bilinear form. Without loss of generality, we analyze the case that both many-body states are many-body standard basis states, i.e.,

$$|\Psi\rangle = |\psi_{i_1}\rangle \wedge |\psi_{i_2}\rangle \wedge \cdots \wedge |\psi_{i_k}\rangle\,,$$
$$|\Phi\rangle = |\phi_{j_1}\rangle \wedge |\phi_{j_2}\rangle \wedge \cdots \wedge |\phi_{j_k}\rangle\,.$$

Further, we introduce an auxiliary basis $\{|\omega_i\rangle\}_{i=1}^n$ to facilitate the calculations. Note that the auxiliary basis will not affect the results and its choice is arbitrary. We could choose it to be any orthonormal basis in $\mathbb{C}^n$. The auxiliary space spanned by $\{|\omega_i\rangle\}_{i=1}^n$ is denoted as Ω. A linear map $\boldsymbol{u}:\Omega\to\Omega$ is defined as

$$\boldsymbol{u} = \sum_{i,j=1}^{n} \langle\psi_i|\phi_j\rangle\,|\omega_i\rangle\,\langle\omega_j|\,. \tag{22}$$

Using the linear map $\boldsymbol{u}$, the inner product of $|\Psi\rangle$ and $|\Phi\rangle$ admits,

$$\begin{aligned}
\langle\Phi|\Psi\rangle &= (|\psi_{i_1}\rangle \wedge \cdots \wedge |\psi_{i_k}\rangle\,, |\phi_{j_1}\rangle \wedge \cdots \wedge |\phi_{j_k}\rangle)\\
&= \det\begin{pmatrix} \langle\psi_{i_1}|\phi_{j_1}\rangle & \cdots & \langle\psi_{i_1}|\phi_{j_k}\rangle \\ \vdots & \ddots & \vdots \\ \langle\psi_{i_k}|\phi_{j_1}\rangle & \cdots & \langle\psi_{i_k}|\phi_{j_k}\rangle \end{pmatrix}\\
&= \det\begin{pmatrix} \langle\omega_{i_1}|\,\boldsymbol{u}\,|\omega_{j_1}\rangle & \cdots & \langle\omega_{i_1}|\,\boldsymbol{u}\,|\omega_{j_k}\rangle \\ \vdots & \ddots & \vdots \\ \langle\omega_{i_k}|\,\boldsymbol{u}\,|\omega_{j_1}\rangle & \cdots & \langle\omega_{i_k}|\,\boldsymbol{u}\,|\omega_{j_k}\rangle \end{pmatrix}\\
&= (|\omega_{i_1}\rangle \wedge \cdots \wedge |\omega_{i_k}\rangle\,, \boldsymbol{u}\,|\omega_{j_1}\rangle \wedge \cdots \wedge \boldsymbol{u}\,|\omega_{j_k}\rangle)\\
&= (|\omega_{i_1}\rangle \wedge \cdots \wedge |\omega_{i_k}\rangle\,, \wedge\boldsymbol{u}\,|\omega_{j_1}\rangle \wedge \cdots \wedge |\omega_{j_k}\rangle).
\end{aligned} \tag{23}$$

Recall that Q_ψ, Q_ϕ, and Q_ω are the same quantum encoding technique applied to different basis sets. Hence, for two many-body bases constructed by the same selection of one-body bases, their quantum encoding map to the same state representation on quantum computer, i.e., the same bit string representation. More precisely, for two many-body bases, $|\psi_{i_1}\rangle \wedge |\psi_{i_2}\rangle \wedge \cdots \wedge |\psi_{i_k}\rangle$ and $|\omega_{i_1}\rangle \wedge |\omega_{i_2}\rangle \wedge \cdots \wedge |\omega_{i_k}\rangle$, which are constructed by one-body bases of the same indices $i_1, i_2, \ldots, i_k$, their quantum encoded states are the same, i.e.,

$$\boldsymbol{Q}_\psi(|\psi_{i_1}\rangle\wedge|\psi_{i_2}\rangle\wedge\cdots\wedge|\psi_{i_k}\rangle) = \boldsymbol{Q}_\omega(|\omega_{i_1}\rangle\wedge|\omega_{i_2}\rangle\wedge\cdots\wedge|\omega_{i_k}\rangle).$$

Using such a relationship of quantum encoding, we continue deriving (23) as,

$$\begin{aligned}
\langle\Phi|\Psi\rangle &= (|\omega_{i_1}\rangle \wedge \cdots \wedge |\omega_{i_k}\rangle\,, \wedge\boldsymbol{u}\,|\omega_{j_1}\rangle \wedge \cdots \wedge |\omega_{j_k}\rangle)\\
&= (\boldsymbol{Q}_\omega^{-1}\boldsymbol{Q}_\omega\,|\omega_{i_1}\rangle \wedge \cdots \wedge |\omega_{i_k}\rangle\,,\\
&\quad (\wedge\boldsymbol{u})\boldsymbol{Q}_\omega^{-1}\boldsymbol{Q}_\omega\,|\omega_{j_1}\rangle \wedge \cdots \wedge |\omega_{j_k}\rangle)\\
&= (\boldsymbol{Q}_\omega^{-1}\boldsymbol{Q}_\psi\,|\psi_{i_1}\rangle \wedge \cdots \wedge |\psi_{i_k}\rangle\,,\\
&\quad (\wedge\boldsymbol{u})\boldsymbol{Q}_\omega^{-1}\boldsymbol{Q}_\phi\,|\phi_{j_1}\rangle \wedge \cdots \wedge |\phi_{j_k}\rangle)\\
&= (\boldsymbol{Q}_\omega^{-1}\,|\Psi^q\rangle\,, (\wedge\boldsymbol{u})\boldsymbol{Q}_\omega^{-1}\,|\Phi^q\rangle).
\end{aligned} \tag{24}$$

Notice that the quantum encoding map $\boldsymbol{Q}_\omega$ preserves the inner-product, i.e.,

$$\begin{aligned}
&(\boldsymbol{Q}_\omega\,|\omega_{i_1}\rangle \wedge \cdots \wedge |\omega_{i_k}\rangle\,, \boldsymbol{Q}_\omega\,|\omega_{j_1}\rangle \wedge \cdots \wedge |\omega_{j_k}\rangle)\\
=\,&(|\omega_{i_1}\rangle \wedge \cdots \wedge |\omega_{i_k}\rangle\,, |\omega_{j_1}\rangle \wedge \cdots \wedge |\omega_{j_k}\rangle),
\end{aligned}$$

for any ω, and $i_1, \ldots, i_k$, and $j_1, \ldots, j_k$. Therefore, in the last expression in (24), we could multiply both side by $\boldsymbol{Q}_\omega$ and obtain the definition of operator $\Xi(\psi,\phi)$,

$$\langle\Phi|\Psi\rangle = (|\Psi^q\rangle\,, \boldsymbol{Q}_\omega(\wedge\boldsymbol{u})\boldsymbol{Q}_\omega^{-1}\,|\Phi^q\rangle) = \langle\Psi^q|\,\Xi(\psi,\phi)\,|\Phi^q\rangle\,, \tag{25}$$

ARTICLE IN PRESS

where

$$\Xi(\psi,\phi) = \boldsymbol{Q}_\omega(\wedge \boldsymbol{u})\boldsymbol{Q}_\omega^{-1}.$$

In (25), both $|\Phi^q\rangle$ and $|\Psi^q\rangle$ are quantum encoded states, which are constructed by their own quantum circuits. The remaining task in evaluating the inner product $\langle\Phi|\Psi\rangle$ is to construct $\Xi(\psi,\phi)$ as a quantum circuit. From now on, we take $\boldsymbol{Q}_\omega$ here as the Jordan–Wigner mapping J_ω such that the quantum circuits in Section IV A and Section IV B could be reused directly. Then, the quantum circuit for $\Xi(\psi,\phi)$ is exactly the same as that proposed in Section IV B with $u_{ij} = \langle\psi_i|\phi_j\rangle$ and $\{\omega_i\}_{i=1}^n$ being the underlying basis set. More precisely, incorporating the quantum circuit for $\Xi(\psi,\phi)$ as illustrated in Fig. 1 and projecting all ancilla qubits to state $|0\rangle$, we could obtain the quantum state $\Xi(\psi,\phi)\,|\Phi^q\rangle$ on a quantum computer. For a better understanding and comparison between different inner product quantum circuits, we denote $\tilde{\Xi}(\psi,\phi)$ as the block encoding of $\Xi(\psi,\phi)$. For example, for $\Xi(\psi,\phi)$ in Fig. 1, $\tilde{\Xi}(\psi,\phi)$ is the quantum circuit therein without projecting ancilla qubits to $|0\rangle$.

Combining the quantum circuit for $\Xi(\psi,\phi)$ and swap test as in Fig. 7, we obtain our first quantum circuit for $|\langle\Psi|\Phi\rangle|$ as in Fig. 2. Notice that in Fig. 2, the quantum circuit is constructed using $\tilde{\Xi}(\psi,\phi)$, which is the block encoding instead of $\Xi(\psi,\phi)$ itself. Hence, there is no need for post-selection and all measurements are postponed to the end and been measured simultaneously. This quantum circuit only require one extra ancilla qubit for inner product. Instead, we need to measure all ancilla qubits, including those from $\Xi(\psi,\phi)$ and the one from swap test. The probability of $a+1$ ancilla qubits in $|0\rangle$ leads to the absolute value of the desired inner product, $|\langle\Psi|\Phi\rangle|$. Slightly modified quantum circuits could be used to evaluate the real and imaginary part of $\langle\Psi|\Phi\rangle$, and lead to the value of the desired inner product.

The quantum circuit in Fig. 2 evaluates the absolute value of the inner product based on the following equation,

$$\langle\Psi|\Phi\rangle = \langle\Psi^q|\,\Xi(\psi,\phi)\,|\Phi^q\rangle = \langle\Psi^q|\,\langle 0_a|\,\tilde{\Xi}(\psi,\phi)\,|\Phi^q\rangle\,|0_a\rangle\,, \tag{26}$$

where $|0_a\rangle$ denotes the ancilla qubits in the block encoding of $\Xi(\psi,\phi)$. The last equality in (26) holds due to the design of our block encoding, i.e.,

$$\tilde{\Xi}(\psi,\phi)\,|\Phi^q\rangle\,|0_a\rangle = \Xi(\psi,\phi)\,|\Phi^q\rangle \otimes |0_a\rangle + |\perp\rangle\,,$$

where $|\perp\rangle$ is a state orthogonal to the subspace with ancilla qubits in $|0_a\rangle$. Hence, evaluating the inner product does not require any post-selection — we only need to apply the full block-encoding circuit. In Fig. 2, the inner product with $\langle 0_a|$ is carried out by the measurement projection and the inner product with $\langle\Psi^q|$ is carried out by the swap test.

Another alternative quantum circuit for the inner product is based on the Hadamard test. Here we consider a slightly different setting. Suppose that we have quantum circuits U_Ψ and U_Φ for preparing states $|\Psi^q\rangle$ and $|\Phi^q\rangle$, respectively, i.e.,

$$|\Psi^q\rangle = U_\Psi\,|0_n\rangle\,,\ \text{and}\ \ |\Phi^q\rangle = U_\Phi\,|0_n\rangle\,.$$

Under the VQE framework, U_Ψ and U_Φ are known from parameterized ansatz quantum circuits. Then, the inner product admits,

$$\begin{aligned}\langle\Phi|\Psi\rangle &= \langle\Psi^q|\,\langle 0_a|\,\tilde{\Xi}(\psi,\phi)\,|\Phi^q\rangle\,|0_a\rangle \\ &= \langle 0_{n+a}|\,(U_\Psi^\dagger \otimes I_a)\tilde{\Xi}(\psi,\phi)(U_\Phi \otimes I_a)\,|0_{n+a}\rangle\,.\end{aligned}$$

The quantum circuit to evaluate the real part of $\langle\Phi|\Psi\rangle$ is given in Fig. 3, where the controlled-$(U_\Psi^\dagger \otimes I_a)$ and controlled-$(U_\Phi \otimes I_a)$ are simplified by the controlled-$U_\Psi^\dagger$ and controlled-U_Φ respectively. A simple modification leads to the quantum circuit for the imaginary part of $\langle\Psi|\Phi\rangle$. When the adjoint of the ansatz circuit is not favored, inner product quantum circuits proposed in [69] could be used as an alternative to the Hadamard test.

DATA AVAILABILITY

No datasets were generated or analyzed during the current study.

ACKNOWLEDGMENTS

The work of J.B. and J.L. are supported by the US National Science Foundation under awards CHE-2037263 and DMS 2309378. G.Z. and Y.L. are supported in part by the National Natural Science Foundation of China (12271109) and the Shanghai Pilot Program for Basic Research-Fudan University 21TQ1400100 (22TQ017).

AUTHOR CONTRIBUTIONS

G.Z., J.L., Y.L., and J.B. conceived of the presented idea. G.Z. developed the mathematical theory and performed the computations. All authors (G.Z., J.L., Y.L., and J.B.) verified the analytical methods. J.L. and Y.L. supervised the findings of this work. All authors (G.Z., J.L., Y.L., and J.B.) discussed the results and contributed to the final version of the manuscript. All authors have read and approved the manuscript.

COMPETING INTERESTS

The authors declare no Competing Financial or Non-Financial Interests.

ARTICLE IN PRESS

REFERENCES

[1] A. Peruzzo, J. McClean, P. Shadbolt, M.-H. Yung, X.-Q. Zhou, P. J. Love, A. Aspuru-Guzik, and J. L. O'Brien, A variational eigenvalue solver on a photonic quantum processor, Nature Communications **5**, 4213 (2014).

[2] B. Bauer, D. Wecker, A. J. Millis, M. B. Hastings, and M. Troyer, Hybrid quantum-classical approach to correlated materials, Physical Review X **6**, 031045 (2016), pRX.

[3] A. Kandala, A. Mezzacapo, K. Temme, M. Takita, M. Brink, J. M. Chow, and J. M. Gambetta, Hardware-efficient variational quantum eigensolver for small molecules and quantum magnets, Nature **549**, 242 (2017).

[4] M. Cerezo, A. Arrasmith, R. Babbush, S. C. Benjamin, S. Endo, K. Fujii, J. R. McClean, K. Mitarai, X. Yuan, and L. Cincio, Variational quantum algorithms, Nature Reviews Physics **3**, 625 (2021).

[5] A. Y. Kitaev, Quantum measurements and the abelian stabilizer problem, arXiv preprint quant-ph/9511026 (1995).

[6] D. S. Abrams and S. Lloyd, Simulation of many-body fermi systems on a universal quantum computer, Physical Review Letters **79**, 2586 (1997), pRL.

[7] D. S. Abrams and S. Lloyd, Quantum algorithm providing exponential speed increase for finding eigenvalues and eigenvectors, Physical Review Letters **83**, 5162 (1998).

[8] M. A. Nielsen and I. L. Chuang, *Quantum Computation and Quantum Information: 10th Anniversary Edition*, 10th ed. (Cambridge University Press, USA, 2011).

[9] I. M. Georgescu, S. Ashhab, and F. Nori, Quantum simulation, Reviews of Modern Physics **86**, 153 (2014).

[10] D. Wecker, M. B. Hastings, N. Wiebe, B. K. Clark, C. Nayak, and M. Troyer, Solving strongly correlated electron models on a quantum computer, Phys. Rev. A **92**, 062318 (2015).

[11] I. D. Kivlichan, J. R. McClean, N. Wiebe, C. Gidney, A. Aspuru-Guzik, G. K.-L. Chan, and R. Babbush, Quantum simulation of electronic structure with linear depth and connectivity, Physical Review Letters **120**, 110501 (2018).

[12] R. Babbush, N. Wiebe, J. McClean, J. McClain, H. Neven, and G. K.-L. Chan, Low-depth quantum simulation of materials, Physical Review X **8**, 10.1103/physrevx.8.011044 (2018).

[13] J. C. Slater, Note on hartree's method, Physical Review **35**, 210 (1930).

[14] J. C. Slater, A simplification of the hartree-fock method, Physical review **81**, 385 (1951).

[15] C. C. J. Roothaan, Self-consistent field theory for open shells of electronic systems, Reviews of Modern Physics **32**, 179 (1960), rMP.

[16] D. Vautherin and D. t. Brink, Hartree-fock calculations with skyrme's interaction. i. spherical nuclei, Physical Review C **5**, 626 (1972).

[17] E. J. Baerends, D. Ellis, and P. Ros, Self-consistent molecular hartree—fock—slater calculations i. the computational procedure, Chemical Physics **2**, 41 (1973).

[18] E. R. Johnson and A. D. Becke, A post-hartree-fock model of intermolecular interactions, The Journal of chemical physics **123** (2005).

[19] F. Neese, F. Wennmohs, A. Hansen, and U. Becker, Efficient, approximate and parallel hartree–fock and hybrid dft calculations. a 'chain-of-spheres' algorithm for the hartree–fock exchange, Chemical Physics **356**, 98 (2009).

[20] P. Siegbahn, A. Heiberg, B. Roos, and B. Levy, A comparison of the super-ci and the newton-raphson scheme in the complete active space scf method, Physica Scripta **21**, 323 (1980).

[21] P. E. Siegbahn, J. Almlöf, A. Heiberg, and B. O. Roos, The complete active space scf (casscf) method in a newton–raphson formulation with application to the hno molecule, The Journal of Chemical Physics **74**, 2384 (1981).

[22] B. O. Roos, P. R. Taylor, and P. E. M. Sigbahn, A complete active space scf method (casscf) using a density matrix formulated super-ci approach, Chemical Physics **48**, 157 (1980).

[23] P. J. Knowles and H.-J. Werner, An efficient second-order mc scf method for long configuration expansions, Chemical Physics Letters **115**, 259 (1985).

[24] D. Zgid and M. Nooijen, The density matrix renormalization group self-consistent field method: Orbital optimization with the density matrix renormalization group method in the active space, The Journal of chemical physics **128**, 144116 (2008).

[25] D. Ghosh, J. Hachmann, T. Yanai, and G. Chan, Orbital optimization in the density matrix renormalization group, with applications to polyenes and β-carotene, The Journal of chemical physics **128**, 144117 (2008).

[26] T. Yanai, Y. Kurashige, D. Ghosh, and G. K.-L. Chan, Accelerating convergence in iterative solution for large-scale complete active space self-consistent-field calculations, International Journal of Quantum Chemistry **109**, 2178 (2009).

[27] J. Olsen, The casscf method: A perspective and commentary, International Journal of Quantum Chemistry **111**, 3267 (2011).

[28] S. Wouters, T. Bogaerts, P. Van Der Voort, V. Van Speybroeck, and D. Van Neck, Communication: Dmrg-scf study of the singlet, triplet, and quintet states of oxo-mn(salen), The Journal of Chemical Physics **140**, 10.1063/1.4885815 (2014).

[29] L. Freitag, S. Knecht, C. Angeli, and M. Reiher, Multireference perturbation theory with cholesky decomposition for the density matrix renormalization group, Journal of Chemical Theory and Computation **13**, 451 (2017), doi: 10.1021/acs.jctc.6b00778.

[30] J. E. T. Smith, B. Mussard, A. A. Holmes, and S. Sharma, Cheap and near exact casscf with large active spaces, Journal of Chemical Theory and Computation **13**, 5468 (2017), doi: 10.1021/acs.jctc.7b00900.

[31] Q. Sun, J. Yang, and G. K.-L. Chan, A general second order complete active space self-consistent-field solver for large-scale systems, Chemical Physics Letters **683**, 291 (2017).

[32] L. Freitag, Y. Ma, A. Baiardi, S. Knecht, and M. Reiher, Approximate analytical gradients and nonadiabatic couplings for the state-average density matrix renormalization group self-consistent-field method, Journal of Chemical Theory and Computation **15**, 6724 (2019), doi: 10.1021/acs.jctc.9b00969.

[33] D. A. Kreplin, P. J. Knowles, and H.-J. Werner, Second-order mcscf optimization revisited. i. improved algorithms for fast and robust second-order casscf

ARTICLE IN PRESS

convergence, The Journal of Chemical Physics **150**, 10.1063/1.5094644 (2019).
[34] D. S. Levine, D. Hait, N. M. Tubman, S. Lehtola, K. B. Whaley, and M. Head-Gordon, Casscf with extremely large active spaces using the adaptive sampling configuration interaction method, Journal of Chemical Theory and Computation **16**, 2340 (2020), doi: 10.1021/acs.jctc.9b01255.
[35] Y. Li and J. Lu, Optimal orbital selection for full configuration interaction (optorbfci): Pursuing basis set limit under budget., Journal of chemical theory and computation (2020).
[36] W. Mizukami, K. Mitarai, Y. O. Nakagawa, T. Yamamoto, T. Yan, and Y.-y. Ohnishi, Orbital optimized unitary coupled cluster theory for quantum computer, Physical Review Research **2**, 033421 (2020).
[37] J. Tilly, P. Sriluckshmy, A. Patel, E. Fontana, I. Rungger, E. Grant, R. Anderson, J. Tennyson, and G. H. Booth, Reduced density matrix sampling: Self-consistent embedding and multiscale electronic structure on current generation quantum computers, Physical Review Research **3**, 033230 (2021).
[38] S. Yalouz, B. Senjean, J. Günther, F. Buda, T. E. O'Brien, and L. Visscher, A state-averaged orbital-optimized hybrid quantum–classical algorithm for a democratic description of ground and excited states, Quantum Science and Technology **6**, 024004 (2021).
[39] J. Bierman, Y. Li, and J. Lu, Improving the accuracy of variational quantum eigensolvers with fewer qubits using orbital optimization, Journal of Chemical Theory and Computation **19**, 790 (2023), doi: 10.1021/acs.jctc.2c00895.
[40] J. Bierman, Y. Li, and J. Lu, Qubit count reduction by orthogonally constrained orbital optimization for variational quantum excited-state solvers, Journal of Chemical Theory and Computation **20**, 3131 (2024), doi: 10.1021/acs.jctc.3c01297.
[41] Y. Shen, X. Zhang, S. Zhang, J.-N. Zhang, M.-H. Yung, and K. Kim, Quantum implementation of the unitary coupled cluster for simulating molecular electronic structure, Physical Review A **95**, 020501 (2017).
[42] A. G. Taube and R. J. Bartlett, New perspectives on unitary coupled-cluster theory, International journal of quantum chemistry **106**, 3393 (2006).
[43] J. Lee, W. J. Huggins, M. Head-Gordon, and K. B. Whaley, Generalized unitary coupled cluster wave functions for quantum computation, Journal of chemical theory and computation **15**, 311 (2018).
[44] J. Romero, R. Babbush, J. R. McClean, C. Hempel, P. J. Love, and A. Aspuru-Guzik, Strategies for quantum computing molecular energies using the unitary coupled cluster ansatz, Quantum Science and Technology **4**, 014008 (2018).
[45] A. Anand, P. Schleich, S. Alperin-Lea, P. W. K. Jensen, S. Sim, M. Díaz-Tinoco, J. S. Kottmann, M. Degroote, A. F. Izmaylov, and A. Aspuru-Guzik, A quantum computing view on unitary coupled cluster theory, Chem. Soc. Rev. **51**, 1659 (2022).
[46] H. F. Trotter, On the product of semi-groups of operators, Proceedings of the American Mathematical Society **10**, 545 (1959).
[47] M. Suzuki, Improved trotter-like formula, Physics Letters A **180**, 232 (1993).
[48] N. Hatano and M. Suzuki, Finding exponential product formulas of higher orders, in *Quantum annealing and other optimization methods* (Springer, 2005) pp. 37–68.
[49] G. Vidal, Efficient classical simulation of slightly entangled quantum computations, Physical review letters **91**, 147902 (2003).
[50] D. Thouless, Stability conditions and nuclear rotations in the hartree-fock theory, Nuclear Physics **21**, 225 (1960).
[51] C.-K. Skylaris, A. A. Mostofi, P. D. Haynes, O. Diéguez, and M. C. Payne, Nonorthogonal generalized wannier function pseudopotential plane-wave method, Physical Review B **66**, 035119 (2002).
[52] C.-K. Skylaris, P. D. Haynes, A. A. Mostofi, and M. C. Payne, Introducing onetep: Linear-scaling density functional simulations on parallel computers, The Journal of chemical physics **122** (2005).
[53] D. Maslov, Linear depth stabilizer and quantum fourier transformation circuits with no auxiliary qubits in finite-neighbor quantum architectures, Phys. Rev. A **76**, 052310 (2007).
[54] M. Reck, A. Zeilinger, H. J. Bernstein, and P. Bertani, Experimental realization of any discrete unitary operator, Phys. Rev. Lett. **73**, 58 (1994).
[55] C. A. Jiménez-Hoyos, R. Rodríguez-Guzmán, and G. E. Scuseria, n-electron slater determinants from nonunitary canonical transformations of fermion operators, Physical Review A **86**, 052102 (2012), pRA.
[56] P.-A. Malmqvist and B. O. Roos, The casscf state interaction method, Chemical Physics Letters **155**, 189 (1989).
[57] J. Pittner, H. Lischka, and M. Barbatti, Optimization of mixed quantum-classical dynamics: Time-derivative coupling terms and selected couplings, Chemical Physics **356**, 147 (2009).
[58] F. Kossoski and P.-F. Loos, State-specific configuration interaction for excited states, Journal of Chemical Theory and Computation **19**, 2258 (2023), doi: 10.1021/acs.jctc.3c00057.
[59] A. Marie and H. G. A. Burton, Excited states, symmetry breaking, and unphysical solutions in state-specific casscf theory, The Journal of Physical Chemistry A **127**, 4538 (2023), doi: 10.1021/acs.jpca.3c00603.
[60] S. Yalouz and V. Robert, Orthogonally constrained orbital optimization: Assessing changes of optimal orbitals for orthogonal multireference states, Journal of Chemical Theory and Computation **19**, 1388 (2023), doi: 10.1021/acs.jctc.2c01144.
[61] S. Saade and H. G. A. Burton, Excited state-specific casscf theory for the torsion of ethylene, Journal of Chemical Theory and Computation **20**, 5105 (2024), doi: 10.1021/acs.jctc.4c00212.
[62] G. Granucci, M. Persico, and A. Toniolo, Direct semiclassical simulation of photochemical processes with semiempirical wave functions, The Journal of Chemical Physics **114**, 10608 (2001).
[63] E. Tapavicza, I. Tavernelli, and U. Rothlisberger, Trajectory surface hopping within linear response time-dependent density-functional theory, Physical Review Letters **98**, 023001 (2007), pRL.
[64] R. Mitrić, U. Werner, and V. Bonačić-Koutecký, Nonadiabatic dynamics and simulation of time resolved photoelectron spectra within time-dependent density functional theory: Ultrafast photoswitching in benzylideneaniline, The Journal of Chemical Physics **129**, 10.1063/1.3000012 (2008).

ARTICLE IN PRESS

[65] L. Du and Z. Lan, An on-the-fly surface-hopping program jade for nonadiabatic molecular dynamics of polyatomic systems: Implementation and applications, Journal of Chemical Theory and Computation **11**, 1360 (2015), doi: 10.1021/ct501106d.

[66] F. Plasser, M. Ruckenbauer, S. Mai, M. Oppel, P. Marquetand, and L. González, Efficient and flexible computation of many-electron wave function overlaps, Journal of chemical theory and computation **12**, 1207 (2016).

[67] A. Gilyén, Y. Su, G. H. Low, and N. Wiebe, Quantum singular value transformation and beyond: exponential improvements for quantum matrix arithmetics, in *Proceedings of the 51st Annual ACM SIGACT Symposium on Theory of Computing*, STOC 2019 (Association for Computing Machinery, New York, NY, USA, 2019) p. 193–204.

[68] S. Lloyd, Universal quantum simulators, Science **273**, 1073 (1996).

[69] J. Bierman, Y. Li, and J. Lu, Quantum orbital minimization method for excited states calculation on a quantum computer, Journal of Chemical Theory and Computation **18**, 4674 (2022).

FIGURE LEGENDS

Figure 1. An example for a nonunitary matrix u of dimension 8 with approximated singular values $\tilde{\sigma}_1 = \tilde{\sigma}_2 = 1$, $1 > \tilde{\sigma}_3 \geq \tilde{\sigma}_4 \geq \tilde{\sigma}_5 > 0$, and $\tilde{\sigma}_6 = \tilde{\sigma}_7 = \tilde{\sigma}_8 = 0$. This quantum circuit is the approximated block encoding of $\wedge \boldsymbol{u}$.

Figure 2. Swap test circuit to calculate the inner-product $|\langle\Phi|\Psi\rangle|$. The absolute value square $|\langle\Phi|\Psi\rangle|^2$ is the probability of all the measurement being $|0\rangle$.

Figure 3. Hadamard test circuit to calculate $\mathrm{Re}\,\langle\Psi|\Phi\rangle$, which could be inferred from the probabilities of the measurement result.

Figure 4. Quantum circuit for $J_\psi U(u;\psi) J_\psi^{-1}$. All gates are their complex conjugates.

Figure 5. Quantum circuit of embedded 2-qubit gate. Ancilla qubit is denoted as a, which is initialized to $|0\rangle$ state. The second qubit q is the working qubit which $\boldsymbol{\nu}$ is acted on.

Figure 6. Block encoding for all $\boldsymbol{\nu}_j$ with $\sigma_j = 0$. Here the ancilla qubit a is initialized to $|0\rangle$ state. Other q_j for $r < j \leq n$ are working qubits corresponding to zero singular values of u.

Figure 7. Swap test circuit to calculate the modulus of the inner-product $|\langle\Phi^q|\Psi^q\rangle|$. The modulus square $|\langle\Phi^q|\Psi^q\rangle|^2$ equals to the probability of the measurement result being $|0\rangle$.

ARTICLE IN PRESS